nature immunology

Asynchronous combinatorial action of four regulatory factors activates *Bcl11b* for T cell commitment

Hao Yuan Kueh[1,4], Mary A Yui[1], Kenneth K H Ng[1], Shirley S Pease[1], Jingli A Zhang[1,4], Sagar S Damle[1,4], George Freedman[1,4], Sharmayne Siu[1], Irwin D Bernstein[2], Michael B Elowitz[1,3] & Ellen V Rothenberg[1]

During T cell development, multipotent progenitors relinquish competence for other fates and commit to the T cell lineage by turning on *Bcl11b*, which encodes a transcription factor. To clarify lineage commitment mechanisms, we followed developing T cells at the single-cell level using *Bcl11b* knock-in fluorescent reporter mice. Notch signaling and Notch-activated transcription factors collaborate to activate *Bcl11b* expression irrespectively of Notch-dependent proliferation. These inputs work via three distinct, asynchronous mechanisms: an early locus 'poising' function dependent on TCF-1 and GATA-3, a stochastic-permissivity function dependent on Notch signaling, and a separate amplitude-control function dependent on Runx1, a factor already present in multipotent progenitors. Despite their necessity for *Bcl11b* expression, these inputs act in a stage-specific manner, providing a multitiered mechanism for developmental gene regulation.

Development of immune progenitors into T cells involves progressive relinquishment of access to alternative fates[1,2]. The final executor of the T lineage commitment transition is the gene *Bcl11b*, whose activation is a lineage-specific landmark in early T cell development. *Bcl11b* has many roles in peripheral T cells[3,4], where it is expressed almost universally, but its initial activation is essential for establishing T cell identity during development[5]. Deletion of *Bcl11b* in progenitors blocks T cell commitment[6,7] and impairs T cell receptor rearrangements[8] and expansion of β-chain-expressing pre–T cells[9]. Its deletion at later stages can cause mature T cells to become natural killer (NK)-like cells[10].

Bcl11b is activated late in the course of initial T cell specification. Upon stimulation by Notch–Delta signals in the thymus, progenitors first transition from an early T progenitor (ETP) stage, identified as c-Kit$^+$ and CD4$^-$CD8$^-$ (double negative 1 (DN1)), to DN2a, where *Bcl11b* activation is first detectable at the population level. DN2a progenitors then transition to DN2b, at which expression of *Bcl11b* is further increased and cells lose the potential to generate NK or dendritic cells[11,12]. The process of *Bcl11b* activation and lineage commitment from the earliest thymus-settling postnatal progenitors spans about 10 d and cell cycles[13], allowing cells to expand substantially before commitment is complete.

Bcl11b activation and T lineage commitment depend on Notch signaling and on an ensemble of transcription factors that include Runx1, TCF-1 (encoded by *Tcf7*) and GATA-3 (refs. 14–17). GATA-3 and TCF-1 are activated by Notch signaling. Runx1, already expressed in hematopoietic stem cells, is upregulated by Notch[15,18–20]. It is possible that these factors all bind the *Bcl11b* locus concurrently to coordinate its activation, as in well-established precedents of combinatorial gene regulation[21,22]. In this case, the timing of *Bcl11b* activation would be controlled by slow accumulation of one or more upstream factors that would need to reach a quorum on the gene locus to cause induction. Alternatively, these factors may collaborate in an asynchronous manner to control *Bcl11b* expression. Work in several systems has shown that some transcription factors act as 'pioneers' and may physically open chromatin around genes to enable subsequent binding of other factors[23,24]. Thus, *Bcl11b* activation could involve temporally separate actions of transcription factors, where some act early to control activation and others act later to maintain expression.

Distinguishing between these models requires isolating cells in distinct gene-expression states and comparing their developmental plasticity. Population-level gene-expression measurements, which average across cell states and temporal stages, are not definitive for this. Therefore, to pinpoint the mechanisms of *Bcl11b* activation and T lineage commitment, we generated a knock-in fluorescent reporter at the *Bcl11b* locus and followed *Bcl11b* activation dynamics at the single-cell level using *in vitro* developmental assays together with flow cytometry and time-lapse live imaging. We show that *Bcl11b* activation coincides with commitment at the single-cell level. To activate this locus, multiple transcription factors have precisely staged, often transient roles. The factors controlling *Bcl11b* expression amplitude

[1]Division of Biology and Biological Engineering, California Institute of Technology, Pasadena, California, USA. [2]Clinical Research Division, Fred Hutchinson Cancer Research Center, Seattle, Washington, USA. [3]Howard Hughes Medical Institute, California Institute of Technology, Pasadena, California, USA. [4]Present addresses: Department of Bioengineering, University of Washington, Seattle, Washington, USA (H.Y.K.), Genentech, South San Francisco, California, USA (J.A.Z.), Department of Bioinformatics, Antisense Drug Discovery, Isis Pharmaceuticals, Carlsbad, California, USA (S.S.D.), and Department of Pediatrics, University of California, San Francisco School of Medicine, San Francisco, California, USA (G.F.). Correspondence should be addressed to H.Y.K. (kueh@uw.edu) or E.V.R. (evroth@its.caltech.edu).

Received 26 January; accepted 14 June; published online 4 July 2016; doi:10.1038/ni.3514

differ from those that license the locus for expression competence, a regulatory strategy that frees the latter to have subsequent roles in mature T cell functional specialization.

RESULTS

Bcl11b-YFP recapitulates Bcl11b expression in T cells

GATA-3, TCF-1, Runx1 and Notch bind to *cis*-regulatory elements of the *Bcl11b* locus[10,15,25–27] (**Supplementary Fig. 1**), and all show evidence for functional roles in *Bcl11b* expression[14,16,17,28,29], but how they collaborate to control *Bcl11b* activation is not understood. To analyze how *Bcl11b* activation and T cell lineage commitment work at the single-cell level, we generated a knock-in fluorescent reporter mouse strain for *Bcl11b* expression. Using standard gene targeting, we inserted a neomycin-resistant (*neo*) internal ribosome entry site (IRES)-mCitrine (YFP) cassette into the 3′ untranslated region of *Bcl11b* in mouse embryonic stem cells (**Supplementary Fig. 2**). We then injected correctly targeted ES cells into blastocyst-stage embryos to generate *Bcl11b*$^{YFP/+}$ mice. This knock-in reporter recapitulated the dynamic regulation of *Bcl11b* in adult T cell progenitors (**Fig. 1a**). The Bcl11b-YFP reporter was undetectable in c-Kit^{hi} DN1 thymocytes (ETPs) and began to be expressed in DN2a thymocytes (**Fig. 1a**), as previously observed[11,25,30]. DN2a progenitors comprised two distinct populations—one in which Bcl11b-YFP expression was not yet detectable and one in which it was (**Fig. 1a**)—suggesting that *Bcl11b* activation occurs after transition to the DN2a stage. Bcl11b-YFP expression increased during stages DN2b and DN3, i.e., up to T cell antigen receptor-β (TCRβ) rearrangement, and was stably maintained in all subsequent stages and major effector T cell subsets but undetectable in B or NK cells (**Fig. 1b**). *Bcl11b*$^{YFP/YFP}$ T cells had approximately twofold higher YFP expression than *Bcl11b*$^{YFP/+}$ cells in all subsets analyzed (**Fig. 1a**,**b**). Together with the unimodal YFP expression in *Bcl11b*$^{YFP/+}$ T cells beyond the DN2a stage, this finding indicated that both *Bcl11b* alleles were activated in the large majority of T cells. Mice with the *neo*-containing *Bcl11b*-YFP knock-in allele were used in all experiments shown here, but *neo* cassette excision from the *Bcl11b*^{YFP} locus did not affect its expression pattern (**Supplementary Fig. 3**).

Bcl11b turns on after DN2a stage entry

Previous analysis of Bcl11b expression has indicated that ETPs differentiate into CD25$^+$ DN2a thymocytes, turn on Bcl11b expression and then downregulate CD44 and c-Kit to enter the DN2b and DN3 stages. To directly verify this developmental sequence, we sorted ETP, Bcl11b-YFP$^-$ DN2a, Bcl11b-YFP$^+$ DN2a and (uniformly) Bcl11b-YFP$^+$ DN2b thymocytes and analyzed their developmental progression on OP9 stromal cells engineered to express the Notch ligand Delta-like 1 (OP9-DL1). OP9-DL1 monolayers serve as an *in vitro* system that supports the early stages of T cell development[31]. After 3 d, ETPs expressed Bcl11b-YFP but only after becoming CD25$^+$ (DN2) (**Fig. 1c**). The majority of Bcl11b-YFP$^-$ DN2a cells turned on *Bcl11b*, and a subset of those downregulated expression of CD44, indicating a transition to the DN2b and DN3 stages (**Fig. 1c**). Thus, *Bcl11b* activation is a discrete regulatory event that occurs after transition into the DN2a stage.

Bcl11b activation coincides with T lineage commitment

Transition of developing thymocytes from DN2a to DN2b coincides with commitment to the T lineage[11]. Loss of alternative potential could occur upon *Bcl11b* activation in DN2a thymocytes or only after transition of Bcl11b-YFP$^+$ DN2a cells to the DN2b stage. To distinguish between these possibilities, we isolated Bcl11b-YFP$^-$ ETP,

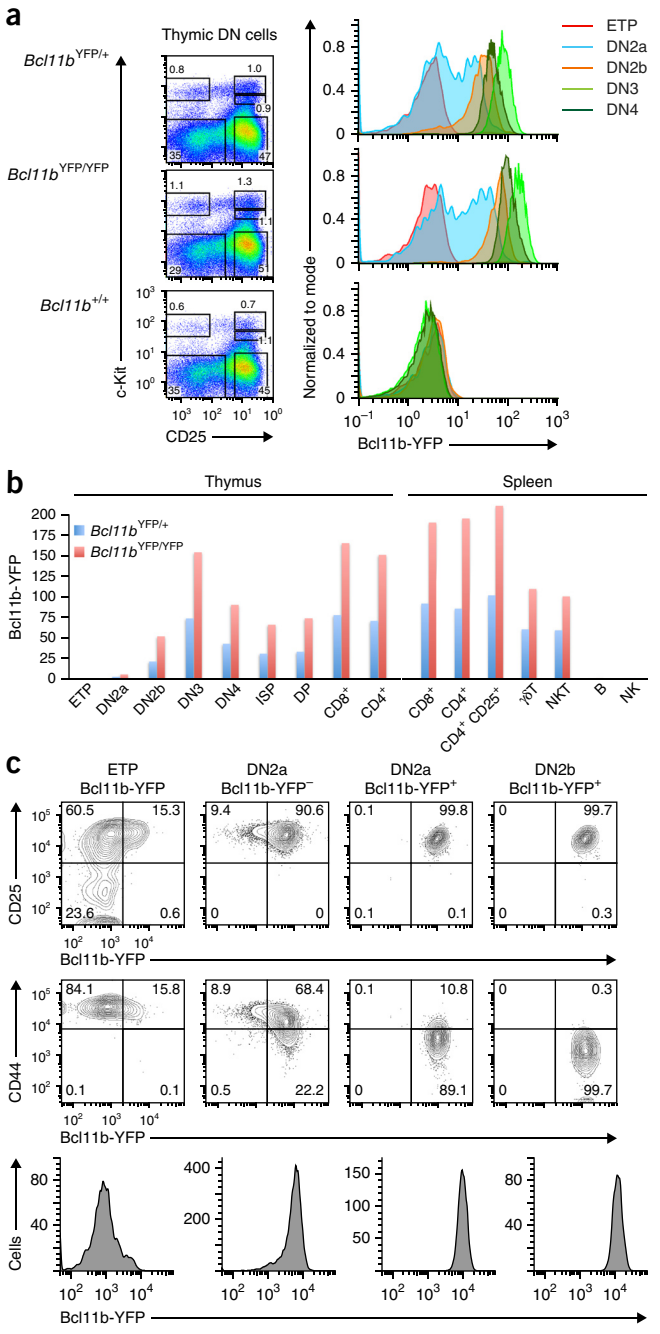

Figure 1 *Bcl11b* expression turns on in developing T cell progenitors and stays on throughout development and maturation. (**a**) Flow cytometry analysis of Bcl11b-YFP expression in DN thymocytes from *Bcl11b*$^{YFP/+}$, *Bcl11b*$^{YFP/YFP}$ and *Bcl11b*$^{+/+}$ mice, showing gates used for defining DN subpopulations (left) and Bcl11b-YFP distributions for those populations (right). (**b**) Mean Bcl11b-YFP levels (arbitrary units) from flow cytometry measurements in various T cell populations from the thymus or spleen in *Bcl11b*-YFP reporter mice. Baseline levels in B and NK cells, which do not express Bcl11b, do not exceed 2.6 on this scale, similar to that of T cells from control C57Bl/6 mice. (**c**) Flow cytometry analysis of T cell developmental progression and Bcl11b-YFP levels in the progeny of sorted DN progenitors, cultured for 3 d on OP9-DL1 monolayers with 5 ng/ml IL-7 and Flt3L. Data are representative of two (**a**,**b**) or three (**c**) independent experiments. Numbers inside plots show percentages of cells within corresponding gates.

Bcl11b-YFP⁻ DN2a, Bcl11b-YFP⁺ DN2a and Bcl11b-YFP⁺ DN2b progenitors from the thymi of wild-type mice and compared their NK cell and DC potentials by culturing them on OP9 cells, which do not stimulate Notch–Delta signaling (**Fig. 2a** and Online Methods). When 300 sorted cells of each subset were cultured in these conditions, Bcl11b-YFP⁻ ETP and Bcl11b-YFP⁻ DN2a thymocytes maintained the potential to differentiate into NK cells and DCs, a result consistent with previous observations, whereas NK and DC potential dropped sharply in Bcl11b-YFP⁺ DN2a cells and was absent in DN2b thymocytes (**Fig. 2a**). This finding was confirmed in limiting dilution cell cultures (**Fig. 2a**). These results indicate that Bcl11b-YFP⁺ DN2a cells are already more restricted than Bcl11b-YFP⁻ DN2a cells in alternative developmental potential.

Molecular context and signature of *Bcl11b* activation

To determine the genome-wide transcriptome changes that accompany the change in developmental potential that accompanies *Bcl11b* activation, we carried out RNA-seq gene-expression analysis using semisynchronized DN subsets from immature bone marrow (BM) progenitors differentiated on OP9-DL1 monolayers (**Fig. 2b**). Cells

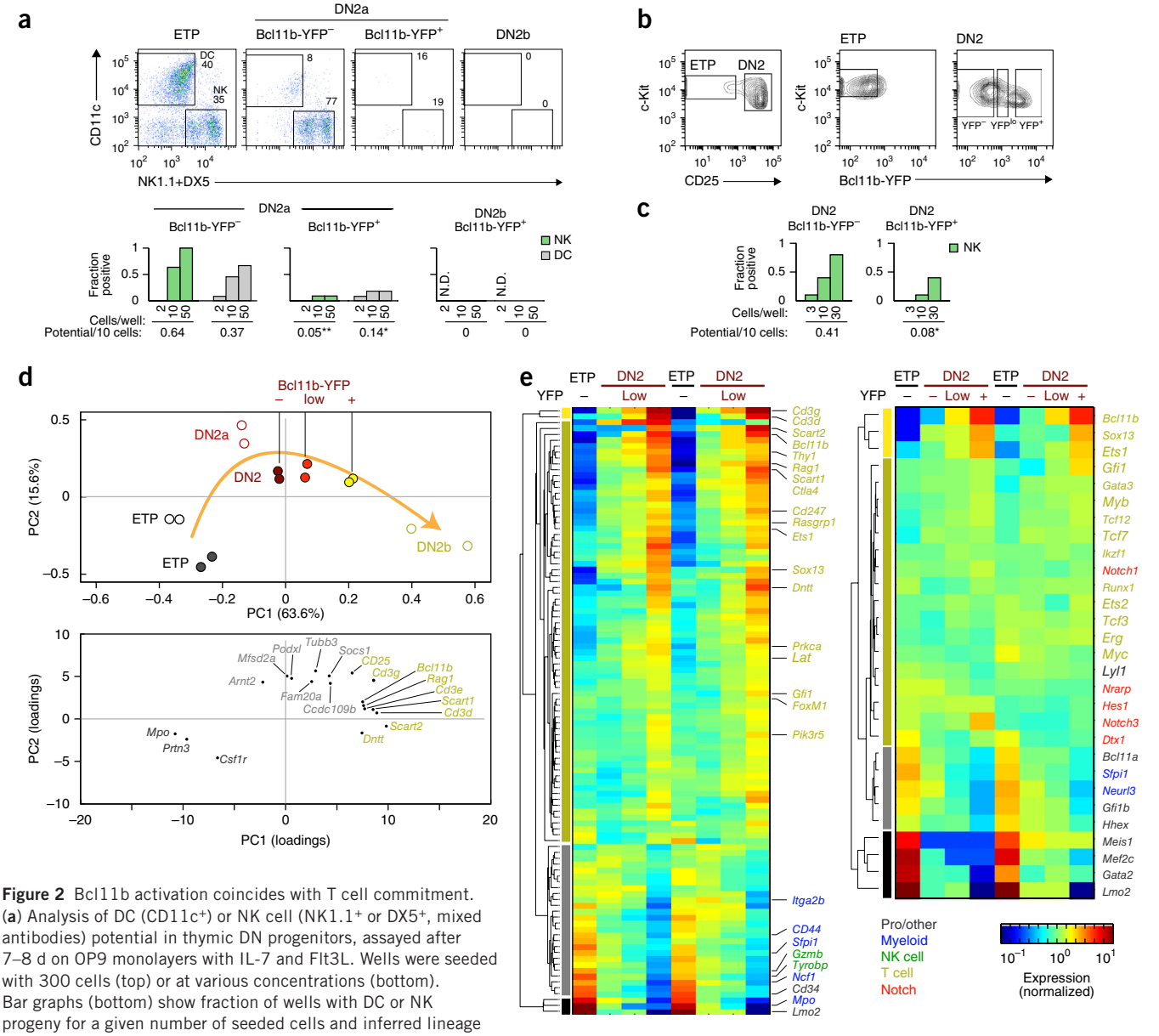

Figure 2 Bcl11b activation coincides with T cell commitment. (**a**) Analysis of DC (CD11c⁺) or NK cell (NK1.1⁺ or DX5⁺, mixed antibodies) potential in thymic DN progenitors, assayed after 7–8 d on OP9 monolayers with IL-7 and Flt3L. Wells were seeded with 300 cells (top) or at various concentrations (bottom). Bar graphs (bottom) show fraction of wells with DC or NK progeny for a given number of seeded cells and inferred lineage potential. $*P = 0.01$; $**P = 0.002$; *z*-test on logistic fit). (**b**–**e**) Transcriptomic analysis of BM DN2 progenitors using RNA-seq. (**b**) Sorting strategy for purifying ETP and DN2 subsets from 7 d BM-progenitor-derived cultures. (**c**) Analysis of developmental potential in BM DN progenitors by limiting dilution assays. $*P = 0.01$; *z*-test on logistic fit. (**d**) Principal component (PC) analysis showing projections along first two PC axes (top) and loadings of the top ten PC genes (bottom). Filled circles represent data from the present study; open circles indicate DN populations from a previous study[25]. Arrow represents T cell developmental trajectory. (**e**) Hierarchical clustering analysis of the expression of genes differentially expressed in Bcl11b-YFP⁻ and Bcl11b-YFP⁺ DN2 cells (left, $q < 0.005$) and selected T cell regulatory genes (right) (**Supplementary Tables 1** and **2**). Data in **a** represent 12, 11 and 12 replicates (for 2, 10 and 50 cells per well, respectively) in one experiment, with similar results for three independent experiments. Data in **c** represent 10 replicates in one experiment, with similar results for two independent experiments. Transcriptomic data (**d**,**e**) represent biological replicates from two experiments.

were sorted after 1 week in culture, when the majority of CD45$^+$ cells were DN2 cells just beginning to activate *Bcl11b*, with a minority remaining c-Kit$^+$CD44$^+$CD25$^-$ ETP-like (henceforth called ETP; populations are described in Online Methods). Similarly to thymic progenitors, BM-derived progenitors showed a reduction in NK cell potential upon *Bcl11b* activation (**Fig. 2c**). Transcriptome analysis showed that the patterns of gene expression in BM-derived DN2 subsets first turning on *Bcl11b* fell into a smooth trajectory in principal component space intermediate between early DN2a cells and DN2b cells (**Fig. 2d**). We also created heat maps of gene expression for the most dynamically changing genes overall and for functionally important transcription factor genes (**Fig. 2e** and **Supplementary Tables 1** and **2a**). As DN2 cells progressed from Bcl11b-YFP$^-$ to Bcl-11b-YFP$^+$, they increased expression of T cell identity genes, including those involved in T cell receptor signaling (*Cd3g*, *Cd3d* and *Lat*) and the recombinase-activating gene *Rag1*, and downregulated genes associated with stem, NK and myeloid cells (**Fig. 2e**), consistent with their reduced lineage plasticity. However, known T cell developmental regulators showed limited expression changes as Bcl11b-YFP expression was turned on (**Fig. 2e**). Many differences were observed between ETP and Bcl11b-YFP$^-$ DN2 progenitors (in expression of *Ets1*, *Tcf7*, *Dtx1*, *Bcl11a*, *Sfpi1*, *Mef2c* and *Lmo2*, $P < 0.005$) (**Supplementary Table 2**), and between Bcl11b-YFP^{lo} and Bcl11b-YFP$^+$ DN2 cells (in *Sox13*, *Ets1* and *Lmo2*, $P < 0.005$ (**Supplementary Table 2**). However, for the same probability cutoff, no significant differences in expression were observed between Bcl11b-YFP$^-$ and Bcl11b-YFP^{lo} cells for regulators other *Bcl11b* itself (**Supplementary Table 2b**). Gene-expression and lineage-potential assays together thus demonstrate that *Bcl11b* activation in individual cells coincides with loss of lineage plasticity and acquisition of a committed T cell state.

Control of *Bcl11b* activation by Notch and IL-7 signaling

Bcl11b is expressed only in the Notch-driven T cell and group 2 innate lymphoid cell (ILC2) programs[32], and chromatin immunoprecipitation studies show that the Notch1 intracellular domain and its associated transcription factor CSL bind to the *Bcl11b* locus[10,26] (**Supplementary Fig. 1**), suggesting that Notch–Delta signaling may regulate *Bcl11b* expression directly. *Bcl11b* activation may also be

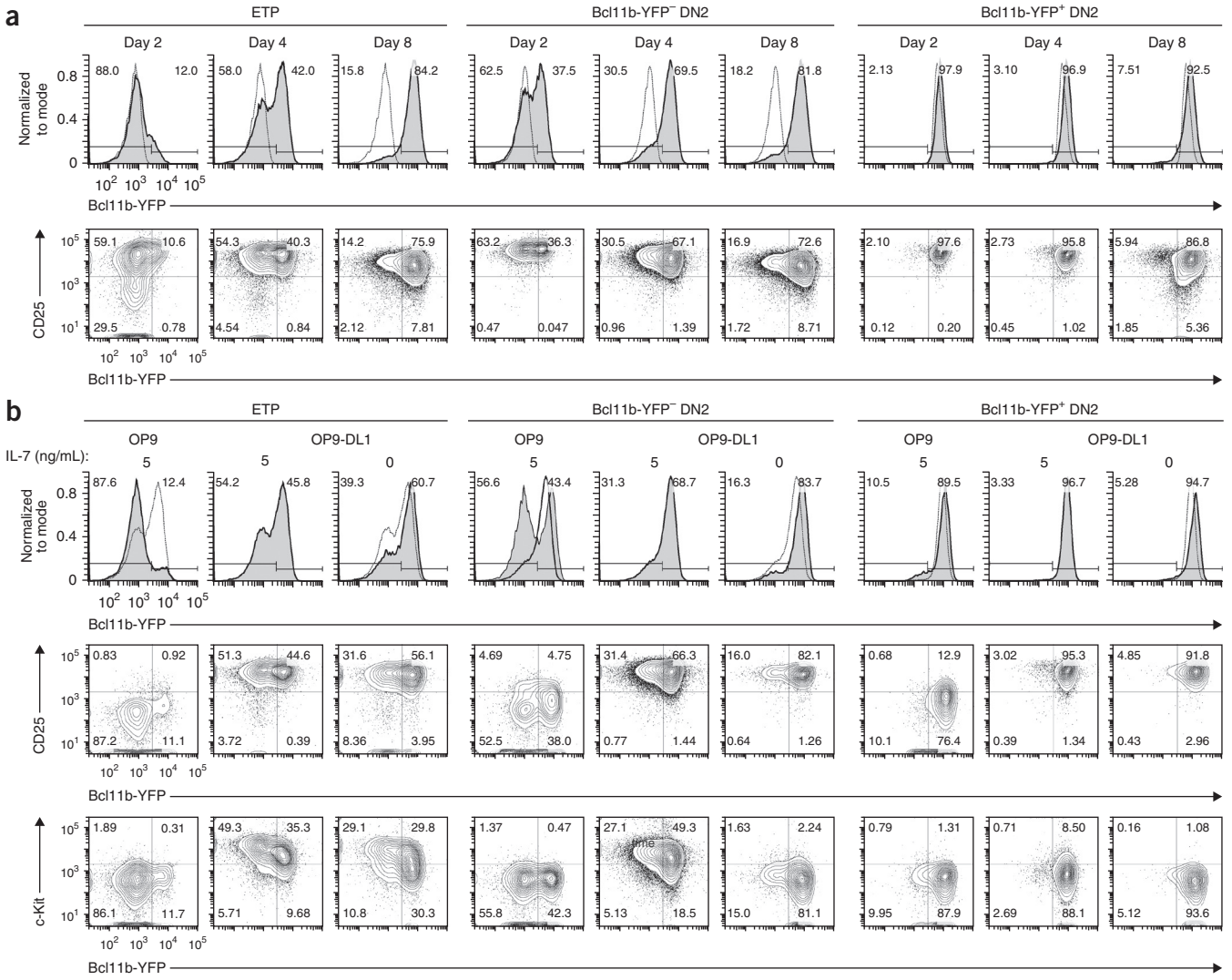

Figure 3 Notch and IL-7 have opposing, stage-specific roles during early T cell development. (**a**) Flow cytometry analysis of Bcl11b-YFP expression for different BM-derived DN progenitor populations after culture on OP9-DL1 stroma for 2, 4 or 8 d. Initial Bcl11b-YFP levels are shown (dotted lines). (**b**) Flow cytometry analysis of BM-derived DN progenitor populations after culture on OP9 or OP9-DL1 with or without IL-7 for 4 d. Results are representative of two (**b**, 5 versus 0 ng/ml IL-7 on OP9-DL1) or five (**a**,**b**, OP9 versus OP9-DL1 culture) independent experiments. Numbers inside plots show percentages of cells within corresponding gates.

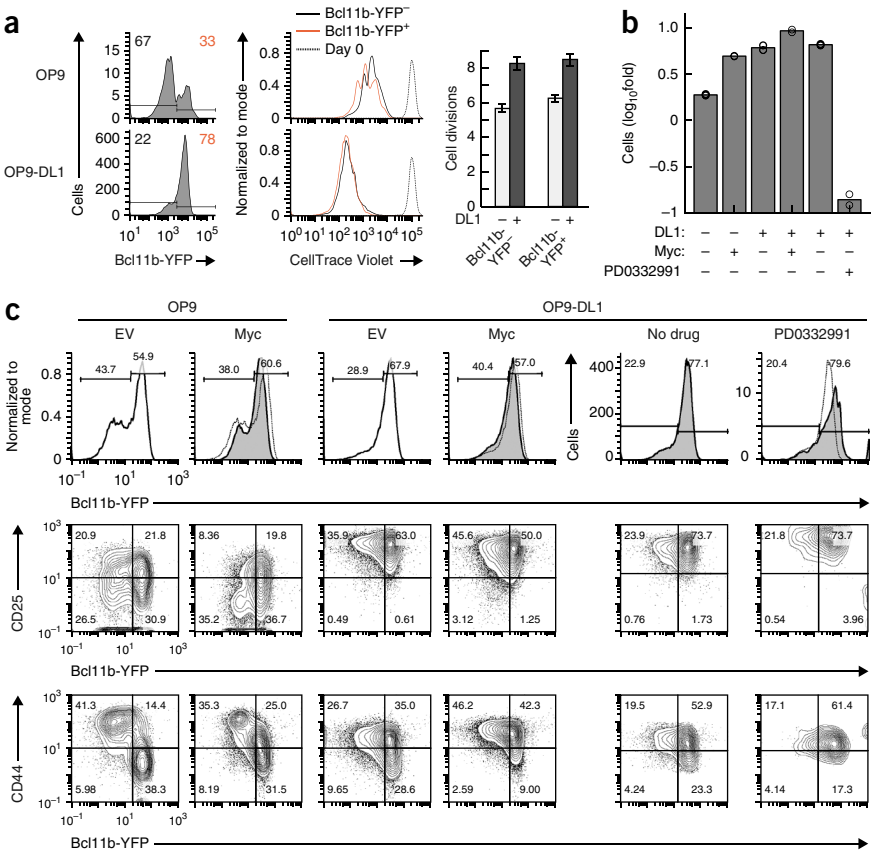

Figure 4 Bcl11b activation is not coupled to Notch-dependent cell proliferation. (**a**) Flow cytometry analysis of Bcl11b expression and cell division kinetics for Bcl11b-YFP⁻ DN2 progenitors stained with CellTrace Violet and cultured for 4 d. The number of cell divisions is given by the log ratio of initial to final CellTrace Violet levels. (**b**,**c**) Flow cytometry analysis (**c**) and quantification (**b**) of BM DN2 progenitors transduced with c-Myc or treated with CDK inhibitor PD0332991 (2.1 μM) and analyzed after 4 d. EV, empty vector. Data in **a** represent mean ± s.d. of three replicates from one experiment, with similar results seen in two independent experiments. Data in **b** represent the mean of two replicates (circles); results in **b** and **c** are representative of two independent experiments. Numbers inside plots show percentages of cells in the corresponding gates.

triggered by removal of IL-7–IL-7R signals[7]. We therefore examined how Notch signals and IL-7 withdrawal affected *Bcl11b* activation in individual BM-derived DN progenitors sorted from OP9-DL1 precultures at different stages of development. Like ETP thymocytes, BM-derived progenitors cultured with OP9-DL1 and IL-7 turned on CD25 to enter the DN2a stage and Bcl11b to enter a committed state (**Fig. 3a**).

Optimal Bcl11b-YFP induction from input BM–derived ETPs depended on Notch signaling and on minimizing IL-7 amounts in culture (**Fig. 3b**), consistent with previous reports[7]. Bcl11b-YFP activation in ETPs was much more efficient on OP9-DL1 than on OP9 monolayers and was most efficient on OP9-DL1 cells in the absence of IL-7 (**Fig. 3b**). ETP cells cultured on OP9 stroma downregulated the stem cell marker c-Kit (**Fig. 3b**), consistent with differentiation into an alternate lineage. However, for cells in which Bcl11b-YFP was already activated, Notch signaling was unnecessary for maintaining Bcl11b expression (**Fig. 3b**). Bcl11b-YFP⁺ cells maintained similar levels of Bcl11b-YFP expression after 4 d of culture on either OP9 or OP9-DL1 stromal cells, whereas CD25 expression was strongly downregulated in Bcl11b-YFP⁺ cells cultured on OP9 compared to OP9-DL1 (**Fig. 3b**). Similarly, IL-7 dosage in the culture had little effect on maintenance of Bcl11b-YFP expression by Bcl11b-YFP⁺ cells (**Fig. 3b**). In Bcl11b-YFP⁻ DN2 cells, IL-7 withdrawal caused a moderate increase in Bcl11b-YFP⁺ frequency while accelerating the downregulation of c-Kit (**Fig. 3b**). However, unlike ETP cells, Bcl11b-YFP⁻ DN2 cells cultured on OP9 showed a split response after 4 d (**Fig. 3b**). Approximately 50% of the Bcl11b-YFP⁻ DN2 cells on OP9 failed to upregulate Bcl11b-YFP, but 50% activated Bcl11b-YFP at least as robustly as on OP9-DL1 (**Fig. 3b**). These results suggest that Notch signaling and IL-7 affect mainly the onset of *Bcl11b* expression rather than its maintenance.

Bcl11b-YFP activation is independent of the cell cycle

The results described above could indicate that Notch signaling activates Bcl11b-YFP expression or that it selectively promotes proliferation of Bcl11b-YFP⁺ cells. To distinguish these options, we measured cell division rates of Bcl11b-YFP⁻ DN2 progeny using CellTrace Violet. Bcl11b-YFP⁻ DN2 cells cultured on OP9-DL1 went through 8 cycles of cell division in 4 d, compared to 5–6 cell cycles on OP9 in the same time interval (**Fig. 4a**). However, 'poised' progenitors that turned on Bcl11b-YFP divided a similar number of times as those remaining Bcl11b-YFP⁻, whether they were cultured on OP9 or OP9-DL1 (**Fig. 4a**). Thus, Notch signaling did not expand *Bcl11b*-expressing cells preferentially.

Still, Notch signaling effects on proliferation raised the possibility that *Bcl11b* activation could require passage through a threshold number of cell cycles, and this could bias detection of *Bcl11b* transcription in favor of Notch-signaled cells. Such a cell-cycle-counting mechanism could be based on a need to remodel chromatin during S phase, reposition it after mitosis or dilute out pre-existing negative regulators and could involve the Notch-induced cell-cycle driver c-Myc[33]. We therefore tested whether the effect of Notch signaling on Bcl11b-YFP activation in Bcl11b-YFP⁻ DN2 cells was altered by overexpression of Myc, which accelerates proliferation, or by treatment with the cyclin-dependent kinase (CDK) inhibitor PD0332991, which slows proliferation[34]. Bcl11b-YFP⁻ DN2 cells retrovirally transduced with Myc proliferated similarly in OP9 and OP9-DL1 cultures (**Fig. 4b**). However, Myc overexpression in cells cultured on OP9 had little impact on *Bcl11b* activation compared to empty vector (**Fig. 4c**). Conversely, PD0332991 blocked proliferation (**Fig. 4b**) but did not substantially impede *Bcl11b* activation by Bcl11b-YFP⁻ DN2 cells (**Fig. 4c**) compared to untreated controls. Thus, a mechanism based on cell-cycle count is not rate limiting for *Bcl11b* induction in Bcl11b-YFP⁻ DN2 cells. Together, these results suggest that Notch signaling directly enhances the rate of *Bcl11b* activation independently of the cell cycle.

Notch signals enhance probabilistic rate of *Bcl11b* induction

To directly visualize effects of Notch on poised Bcl11b-YFP⁻ DN2 progenitors, we sorted Bcl11b-YFP⁻ DN2 cells derived from BM precursors and re-cultured them on OP9 and OP9-DL1 stroma with continuous live imaging (**Supplementary Fig. 4**). When cultured on OP9 stroma, a small fraction of cells turned on Bcl11b-YFP

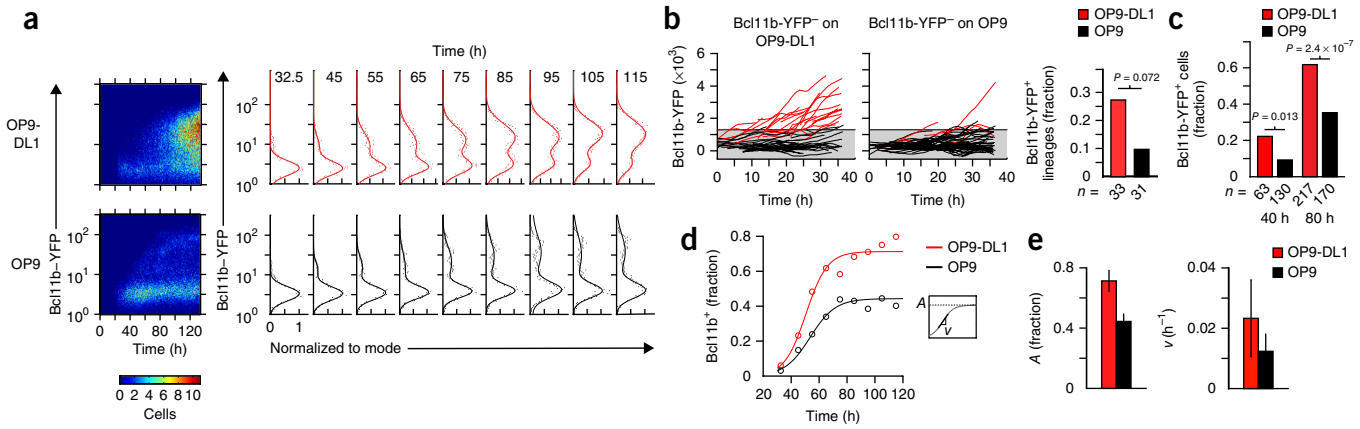

Figure 5 Notch signaling increases the probability of 'all-or-none' Bcl11b activation. (**a**–**d**) Time-lapse imaging analysis of Bcl11b activation dynamics in single Bcl11b-YFP⁻ DN2 progenitors on OP9 or OP9-DL1 monolayers. (**a**) Bcl11b-YFP levels over time in cells cultured on OP9-DL1 (top) or OP9 (bottom) monolayers. Histograms (right) give binned cell data obtained at each time point. Data are shown starting from onset of mCherry expression (t ~25 h). Smooth lines indicate best fits to mixed Gaussian distributions. (**b**) Left and middle, single-cell Bcl11b-YFP time traces on OP9-DL1 or OP9 monolayers, representing pooled data from individually tracked cell lineages. Gray shading indicates background levels of Bcl11b; red traces indicate levels higher than background. Right, fractions of lineages turning on Bcl11b, showing significant increase in Bcl11b-YFP⁺ lineages on OP9-DL1 ($\chi^2 = 3.25$, d.f. = 1). n, number of cells in each group. (**c**) Fractions of Bcl11b-YFP⁺ cells at 40 h and 80 h of culture on OP9-DL1 or OP9 monolayers (40 h, $\chi^2 = 6.1$, d.f. = 1; 80 h, $\chi^2 = 26.7$, d.f. = 1). n, number of cells in each group. (**d**) Time evolution for Bcl11b-YFP⁺ cells, obtained from Gaussian fits in **a**. Smooth curves represent fits to the logistic equation $f(t) = A/[1 + e^{4v(t-\tau)/A}]$ where v = Bcl11b-YFP activation rate, τ = time of half-maximal Bcl11b-YFP activation and A = maximal fraction of Bcl11b-YFP⁺ cells. Inset, graphical depiction of parameters. (**e**) Initial Bcl11b-YFP activation rate (v) and maximal fraction of Bcl11b-YFP⁺ cells (A) from logistic fits, with 95% confidence intervals indicated. Results in **a**, **c**, **d** and **e** were obtained from one experiment; and results in **b** were obtained from a separate experiment in which cells were tracked to 36 h. Bar graph data in **b** and **c** were derived from the indicated number of cells (n). Similar results were seen for a third independent experiment.

expression within the first 2 d of imaging observation (**Fig. 5a**,**b**), and this fraction increased steadily until it reached a plateau value of ~0.4 at about 80–90 h of culture (**Fig. 5c**–**e**). In cells cultured on OP9-DL1 stroma, the fraction of cells that turned on Bcl11b-YFP expression was twice as high as that observed on OP9 after 40 h of culture (**Fig. 5c**), and Bcl11b-YFP induction was accelerated for individual cell lineages during the same period, as assessed by single-cell tracking (**Fig. 5b**). This indicates that Notch signaling has a direct and immediate role in controlling *Bcl11b* activation. Even with continued Notch signaling, the fraction of cells expressing

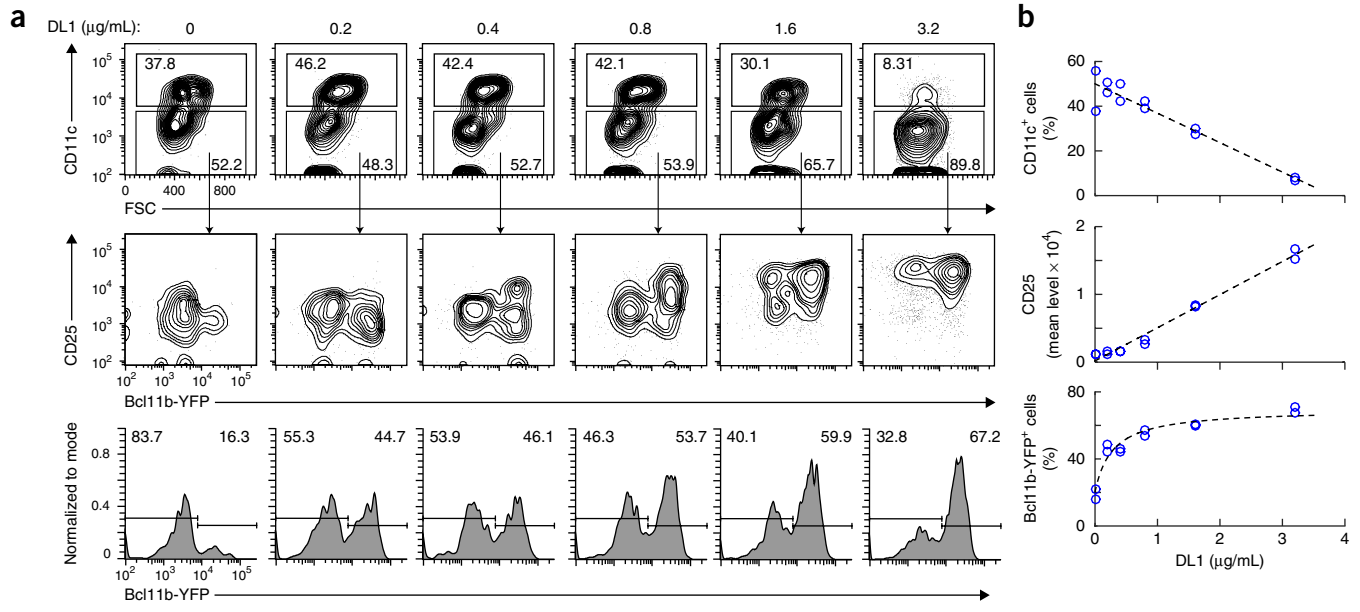

Figure 6 Notch signaling increases Bcl11b activation probability in a dose-dependent manner. (**a**,**b**) Flow cytometry analysis of BM-derived Bcl11b-YFP⁻ DN2 cells cultured on plates with surface-immobilized DL1-Fc (DL1) and analyzed after 4 d. (**a**) Levels of the dendritic cell marker CD11c (top) and CD25 and Bcl11b-YFP levels (middle and bottom) in CD11c⁻ cell populations. (**b**) Percentage of CD11c⁺ DCs (top), mean CD25 expression levels (middle) and Bcl11b-YFP⁺ percentages (bottom) as a function of DL1 dosage. Curves represent best fit to hyperbolic function $f(x) = x/(x + K_e)$ (bottom) or to a straight line (top and middle), which was used due to lack of observable saturation in the concentration series. The DL1 dose required for half-maximal enhancement of Bcl11b activation K_e = 0.28 μg/ml. FSC, forward scatter. Results are representative of four independent experiments. Numbers in plots show cell percentages within corresponding gates.

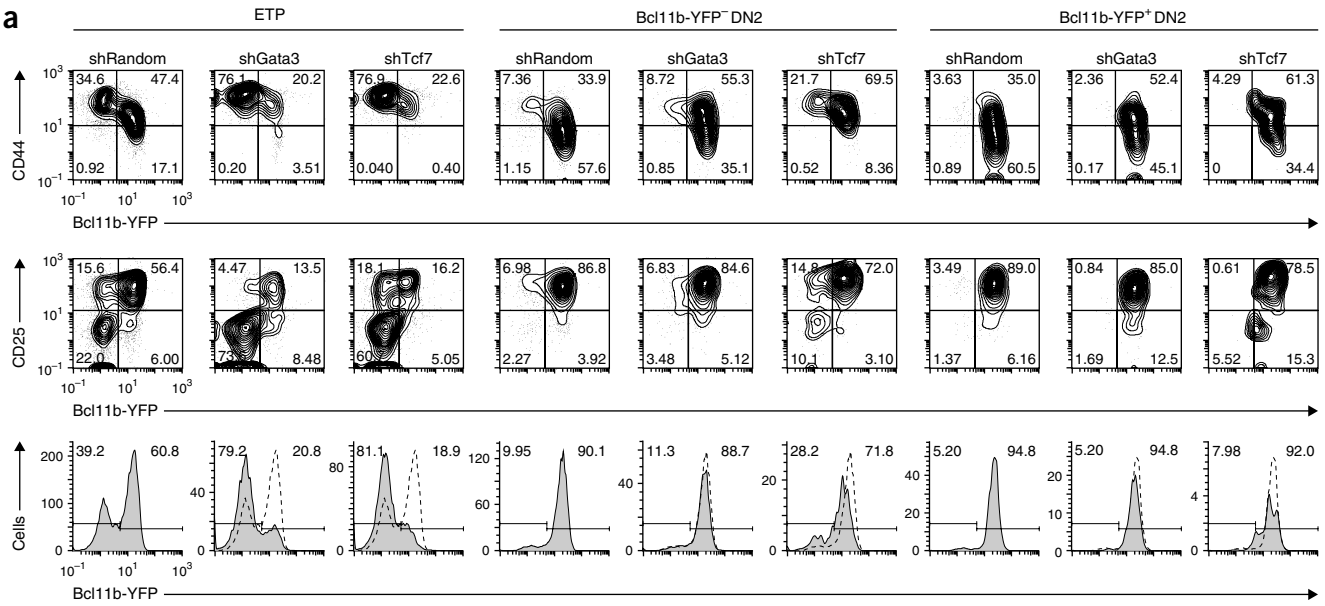

Figure 7 GATA-3 and TCF-1 control initial Bcl11b activation. (**a**,**b**) Flow cytometry analysis of BM-derived DN cells transduced with shGata3 or shTcf7 after further culture on OP9-DL1 monolayers with IL-7 and Flt3L for 5–6 d. (**a**) CD44, CD25 and Bcl11b-YFP levels in ETP and DN2 cells. Dotted lines (bottom) indicate cells transduced with shRandom. (**b**) Fractions of Bcl11b-YFP+ cells from the progeny of the indicated populations. Solid green circles represent data from an alternative *Tcf7*-targeting construct (Online Methods). $*P < 10^{-2}$; $**P < 10^{-4}$, one-tailed unequal variance *t*-test on perturbed versus control conditions. Results in **a** are representative of two independent experiments, and data in **b** show means of *n* replicates from two independent experiments. Numbers in plots show cell percentages within corresponding gates.

Bcl11b appeared to reach a plateau value (~0.8, **Fig. 5d**,**e**), suggesting that DN2 progenitors can eventually lose the ability to activate *Bcl11b* expression, although this possibility requires further investigation. Thus, although Notch signaling is not strictly necessary for *Bcl11b* transcriptional activation, it enhances the probabilistic rate of this event.

To assess the intensity of Notch signaling needed for *Bcl11b* activation, we compared the dose dependence of *Bcl11b* transcriptional activation on Notch signaling to the threshold for two other Notch-dependent responses, CD25 upregulation and restriction of non-T lineage development. We cultured Bcl11b-YFP⁻ DN2 cells in stromal-cell-free conditions for 4 d on tissue culture plates coated with different concentrations of purified DL1-Fc, consisting of the DL1 extracellular domain stabilized as an human IgG1 Fc fusion protein (0–3.2 μg/ml)[35]. The fraction of DN2a cells becoming Bcl11b-YFP+ increased in a dose-dependent manner, reaching a half-maximal value with DL1-Fc at 0.28 μg/ml, as determined by a hyperbolic fit to the data (**Fig. 6a**). Furthermore, increasing DL1-Fc concentrations enhanced the frequency of Bcl11b-YFP+ cells but not the magnitude of Bcl11b-YFP expression in individual cells (**Figs. 3b** and **6**). Similar dose effects were observed upon pharmacological inhibition of Notch signaling by a γ-secretase inhibitor (**Supplementary Fig. 5**). Bcl11b-YFP could be fully activated in a major subset of DN2 cells cultured with DL1-Fc at concentrations that did not sustain CD25 expression or suppress transdifferentiation to CD11c+ DCs (**Fig. 6b**). Thus, *Bcl11b* activation requires a lower Notch signal compared to that required to regulate these other processes.

GATA-3 and TCF-1 control poising of *Bcl11b* for activation

The lower threshold for Notch signals to induce Bcl11b-YFP in DN2a cells compared to ETPs suggested that another rate-limiting factor collaborates with Notch at the DN2a stage to promote Bcl11b-YFP activation. Such factors could be activated by Notch signaling before or coincident with Bcl11b-YFP activation. Our transcriptome analyses showed few if any regulatory gene candidates, other than *Bcl11b* itself, with increased expression between Bcl11b-YFP⁻ DN2 and Bcl11b-YFP^{lo} DN2 (**Fig. 2e** and **Supplementary Table 2b**), although it is possible that their activity or expression is modulated post-transcriptionally. Therefore, we examined the roles of T cell transcription factors implicated previously by genetic evidence, namely GATA-3, TCF-1 and Runx factors in complex with core-binding factor-β (Runx–CBFβ).

The T cell–specific factors GATA-3 and TCF-1 are activated by Notch signaling in the ETP stage, before *Bcl11b* activation[36,37]. To determine how and when these factors are needed for *Bcl11b* expression, we knocked down their expression in progenitors at different developmental stages using small hairpin RNA (shRNA) constructs validated in ETP and DN2 cells[17] (**Supplementary Fig. 6**). Progeny of ETP cells transduced with *Gata3*-targeting shRNA (shGata3) or shTcf7 showed severely inhibited expression of Bcl11b-YFP compared to progeny of cells transduced with a nontargeting control (shRandom) (**Fig. 7**). GATA-3 and TCF-1 knockdown in ETP cells reduced mainly the percentages of Bcl11b-YFP+ cells in their descendants rather than the amount of Bcl11b-YFP expressed per cell (**Fig. 7a**), as with the effects of Notch inhibition. Production of CD25+ cells was also reduced, as expected[15,16,19] (**Fig. 7a**), consistent with an early developmental block. Although some of the cells acquired a DN2 phenotype, TCF-1 knockdown further reduced the fraction of DN2 cells that activated Bcl11b-YFP.

However, the effect on Bcl11b-YFP activation was smaller in Bcl11b-YFP⁻ DN2a cells transduced with shGata3 or shTcf7 than in ETPs (**Fig. 7**). Knockdown of GATA-3 from the DN2a stage on had no detectable effects on Bcl11b-YFP activation. In DN2a cells, TCF-1 knockdown effectively lowered a barrier to DC transdifferentiation (**Supplementary Fig. 7a**) but only mildly impeded Bcl11b-YFP induction

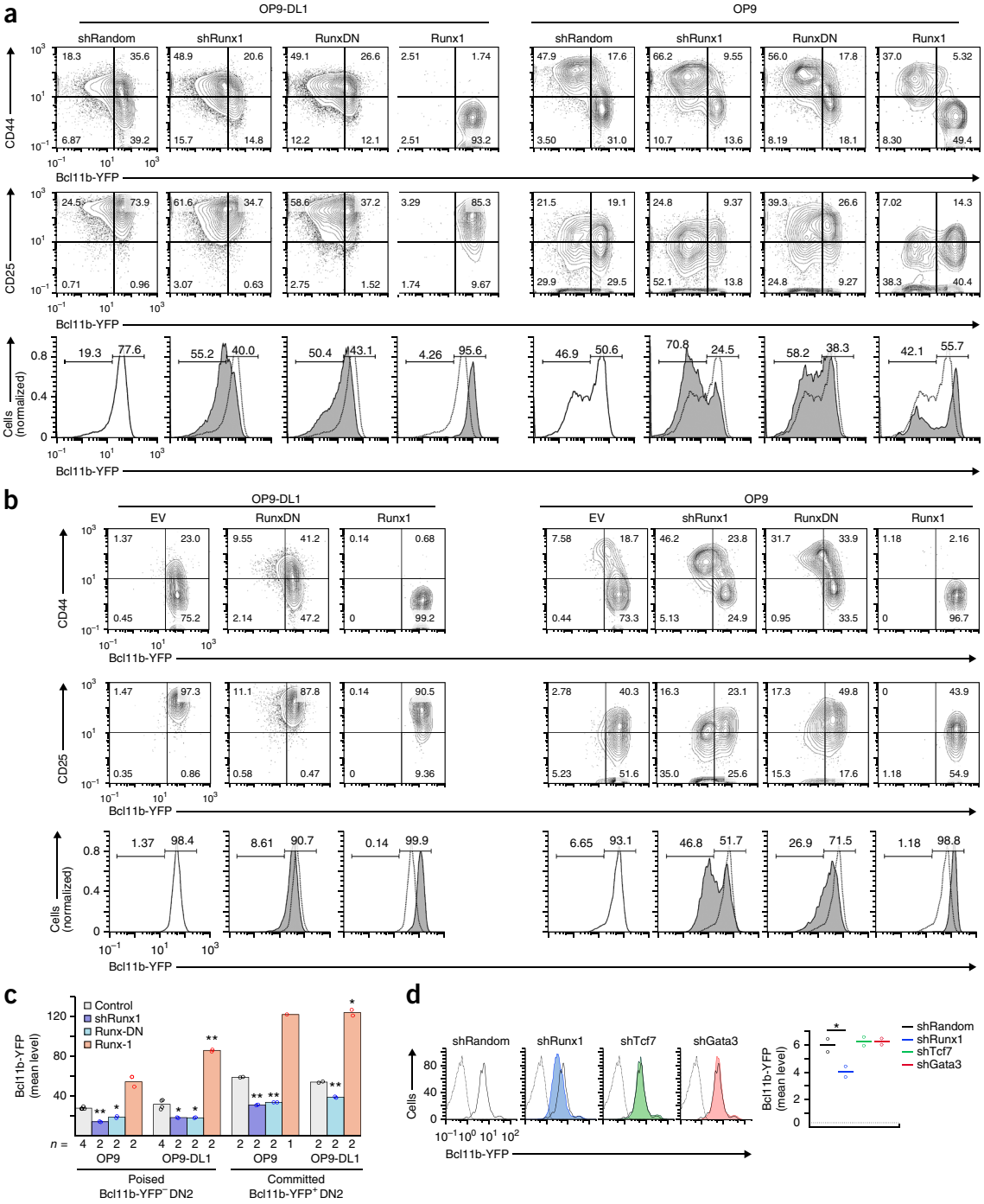

Figure 8 Runx1 controls Bcl11b expression amplitude. (**a**,**b**) Flow cytometry analysis of CD44, CD25 and Bcl11b-YFP levels in Bcl11b-YFP⁻ DN2 cells (**a**) or Bcl11b-YFP⁺ DN2 cells (**b**) transduced with Runx constructs and cultured on OP9-DL1 or OP9 monolayers for 4 d. CD44, CD25 and Bcl11b-YFP levels are shown for initial Bcl11b-YFP⁻ DN2 cells (**a**) or Bcl11b-YFP⁺ DN2 cells (**b**). EV, empty vector. Dotted lines in histograms (bottom) indicate Bcl11b-YFP levels in unperturbed cells. (**c**) Mean Bcl11b-YFP levels under various Runx perturbation conditions. Control, EV or shRandom-transduced cells. $*P < 0.05$; $**P < 0.01$, two-tailed unequal variance *t*-test. (**d**) Flow cytometry analysis and quantification of Bcl11b-YFP expression in CD8⁺ T cells activated with anti-TCRβ and anti-CD28, transduced with shRNA constructs and cultured for 3 d (**Supplementary Fig. 8**). Solid black lines indicate cells transduced with shRandom; dotted lines indicate nonfluorescent T cells (top). $*P < 0.05$, one-tailed unequal variance *t*-test. Results in **a** and **b** are representative of two (Runx, shRunx1) or three (Runx-DN) independent experiments, and data in **c** represent means of *n* replicates from one experiment. Data in **d** represent means of two replicates from one experiment; results are representative of two independent experiments. Numbers in plots show cell percentages within corresponding gates.

compared to cells transduced with shRandom controls (**Fig. 7**). By the DN2b stage, shGata3 and shTcf7 transduction had no effect on Bcl11b-YFP expression compared to shRandom (**Fig. 7b** and **Supplementary Fig. 8**), consistent with reported RNA expression data[38,39]. Conversely, TCF-1 overexpression did not affect Bcl11b-YFP expression in ETP or DN2 cells (**Supplementary Fig. 7b**), suggesting that physiological levels of TCF-1 in ETP or DN2 cells are sufficient for maximum *Bcl11b* induction. These results indicate that GATA-3 and TCF-1 together control entry of cells into a state poised for *Bcl11b* activation but are largely dispensable for maintaining *Bcl11b* expression after commitment.

Runx1 controls *Bcl11b* expression amplitude

We next investigated how the amplitude of *Bcl11b* expression is controlled. Because Runx–CBFβ transcriptional complexes are vital for development of T cells past the DN2 stage[14,40], Runx binding sites are prominent in the *cis*-regulatory regions of *Bcl11b*[28] and germline CBFβ dose reduction severely affects *Bcl11b* expression[14], we tested whether Runx has a role in regulating *Bcl11b* transcription. We transduced Bcl11b-YFP$^-$ DN2 or Bcl11b-YFP$^+$ DN2 progenitors with shRunx1, a pan-Runx dominant-negative (Runx-DN) construct[41] to inhibit Runx activity or a full-length Runx1 cDNA to elevate Runx1 activity and assessed the impacts on the magnitude of Bcl11b-YFP expression after 4 d (**Fig. 8a**,**b**). shRunx1 downshifted the distribution of Bcl11b-YFP expression compared to shRandom or empty vector, whereas Runx1 overexpression shifted Bcl11b-YFP expression up, both during Bcl11b-YFP induction (**Fig. 8a**) and in cells that were already Bcl11b-YFP$^+$ (**Fig. 8b**). Runx-DN had similar but milder effects in both cell types, suggesting that Runx family members other than Runx1 have only minor roles in *Bcl11b* expression. shRunx1 transduction also affected Bcl11b-YFP expression in descendants both of Bcl11b-YFP$^-$ DN2 (**Fig. 8a**,**c**) and of Bcl11b-YFP$^+$ DN2 cells (**Fig. 8b**,**c**) in the absence of Notch signaling, indicating that Runx1 supports the Notch-independent phase of *Bcl11b* expression as well.

To determine whether the roles established for Runx1, TCF-1 and GATA-3 during commitment persist, we examined their effects on Bcl11b-YFP expression in mature T cells. Knockdown of Runx1, but not TCF-1 or GATA-3, in activated, mature peripheral T cells reduced Bcl11b-YFP expression compared to control-transduced cells, both in CD8$^+$ (**Fig. 8d**) and in CD8$^-$ T cells (**Supplementary Fig. 8**). These data show that Runx1 has a role distinct from that of Notch, GATA-3 or TCF-1 and controls the magnitude of *Bcl11b* expression even after T cells leave the thymus.

DISCUSSION

Bcl11b is induced from a silent, repressed state to become fully expressed during commitment between stages DN2a and DN2b. Although further modulated according to effector lineage and activation state[3,4], *Bcl11b* is permanently expressed in all T cells, where it upholds T cell identity and suppresses NK fate[3,5]. Here we used a fluorescent *Bcl11b* reporter allele to show that the silence of *Bcl11b* in early ETPs is functionally different from its poised quiescence in early DN2a cells before its dramatic activation during the T lineage commitment transition. We show that Notch signaling, GATA-3, TCF-1 and Runx1 have distinct, stage-specific roles in controlling this watershed regulatory event. Notch–Delta signaling enhances the likelihood of switch-like *Bcl11b* activation from poised progenitors but is dispensable in sustained *Bcl11b* expression. GATA-3 and TCF-1 control entry into a state poised for *Bcl11b* activation but are also unnecessary for stable expression of *Bcl11b*. Thus, Notch, GATA-3 and TCF-1 primarily act permissively. Notably, both GATA-3 and TCF-1 are activated by Notch signaling, suggesting a double feed-forward network circuit architecture for commitment control. In contrast, Runx1 continuously affects *Bcl11b* expression magnitude with or without Notch signals, indicating an independent role in controlling *Bcl11b* expression after locus activation. Thus, multiple transcription factors, all of which are necessary for T cell generation, collaborate asynchronously to establish cellular identity, and single-cell tracking clearly distinguishes the mechanisms they use to poise cells for commitment from those to execute and maintain lineage-specific gene expression.

Collaboration of multiple transcription factors is fundamental for establishing distinct cell type identities during multicellular organismal development[42] and is also essential for artificial cell fate reprogramming[43,44]. In classical models of developmental gene regulation, it is often assumed that combinatorial function reflects synchronous transcription factor action at *cis*-regulatory DNA elements of target genes[21,22]. However, it is not clear whether all co-occupancy reflects synchronous transcription factor function. In a growing number of systems, lineage-specifying transcription factors are seen to act as 'pioneers', binding early to physically open up developmental gene loci and enable subsequent binding of other factors[23,24]. These pioneer factors need not work coordinately with other factors and may act transiently to generate lasting effects on gene expression[23].

Our results suggest that GATA-3 and TCF-1, which turn on early in ETP cells, may act to poise *Bcl11b* for activation at a later stage. Once the *Bcl11b* locus is poised in Bcl11b-YFP$^-$ DN2 cells, it then transitions to an active state in a Notch-dependent, IL-7-restrained manner and then sustains expression through active regulation by Runx1. In this model, the combinatorial requirement for Notch, GATA-3 and TCF-1 makes *Bcl11b* induction possible only along a narrow range of developmental tracks: the T cell program and the ILC2 program[32]. By the time cells reach Bcl11b-YFP$^-$ DN2 stage, they are 'licensed' for *Bcl11b* activation, thus harboring a potential for activating *Bcl11b* that ETP cells lack. This licensing function could be related to 'pioneering' or locus opening[23,24] and is distinctive in that individual mediators of licensing can be later removed without affecting expression. An alternative interpretation is that GATA-3 and TCF-1 regulate *Bcl11b* indirectly through a later-acting intermediate factor, but the paucity of major regulatory changes concomitant with *Bcl11b* activation disfavors this possibility. When the *Bcl11b* locus is licensed for activation in poised (Bcl11b-YFP$^-$ DN2) cells, activation still takes 2–4 d; these slow kinetics could involve a rate-limiting transition of the locus from an inactive to an active chromatin state, potentially through slow removal of repressive histone marks, DNA demethylation or translocation of the gene locus from the nuclear lamina[25,28,45]. Once the *Bcl11b* locus is activated, its magnitude of expression is sustained by Runx factors. Although Runx factors are expressed from a much earlier stage, they may not be able to reach the relevant sites in the *Bcl11b* gene until after the licensing process is complete, possibly owing to the initially repressed state of the *Bcl11b* locus[28].

In contrast to findings in other genes, the mechanisms controlling the competence of *Bcl11b* to be turned on are thus distinct from those controlling its expression levels. This distinction is revealed only at the single-cell level. The hit-and-run licensing functions performed by Notch, GATA-3 and TCF-1 are separable from the continuous magnitude control by Runx1. We speculate that this separation is a key to potential developmental importance. The same factors that work together to create the T cell identity in progenitors work divergently in later effector T cell subsets. All of these cells need *Bcl11b*, but Notch signaling is shut down in most naive T cells, and TCF-1 and GATA-3 work together to control type 2 helper T (T_H2) cell differentiation in CD4$^+$ T cells, but the TCF-1/GATA-3 ratio is tipped one way in CD8$^+$ T effector cells and

in the opposite way in regulatory T cells. We propose that these cells all continue to express *Bcl11b* because they express Runx1 or other Runx family members and share the developmental history of passing through the lineage-specific licensing process studied here. Making locus opening difficult but irreversible and using different factors to modulate levels enables T cells to reuse these factors in multiple contexts. Given that transcription factors are typically deployed multiple times in multicellular organism development, we speculate that similar mechanisms might underlie regulation in other systems as well.

METHODS

Methods and any associated references are available in the online version of the paper.

Accession codes. Gene Expression Omnibus: raw sequence reads, normalized expression, GSE76606.

Note: Any Supplementary Information and Source Data files are available in the online version of the paper.

ACKNOWLEDGMENTS

We thank M. Lerica Gutierrez Quiloan for assistance with mouse genotyping and maintenance; N. Verduzco and I. Soto for animal husbandry; J. Longmate for help with statistical analysis of alternate-lineage-potential experiments; R.A. Diamond, K. Beadle, J. Grimm, D. Perez and J. Verceles for cell sorting; N. Feng for initial flow cytometric analysis; J. Hahn for advice on BAC recombineering; S. Qin for assistance with qPCR experiments; X.Wang for performing pilot studies with microwell arrays; and J. Ungerbäck for assistance with visualizing genome track data. We also thank A. Bhandoola, L. Xu and W. Pear (University of Pennsylvania); J. Telfer (University of Massachusetts) and N. Masuyama (University of Tokyo) for constructs. This work was funded by a CRI/Irvington Postdoctoral Fellowship and a US National Institutes of Health (NIH) K99/R00 Award (K99HL119638A) to H.Y.K.; a California Institute for Regenerative Medicine Bridges to Stem-Cell Research award to K.K.H.N. (TB1-01176); NIH grants to E.V.R. (R01 AI083514, R01 AI095943, RC2 CA148278, R33 HL089123, R01 CA90233 and R01 HL119102) and M.A.Y. (R01 AI064590); NIH/HHS grant U01HL100395 (I.D.B.); the Albert Billings Ruddock Professorship to E.V.R.; and the Al Sherman Foundation and the Louis A. Garfinkle Memorial Laboratory Fund to E.V.R.'s lab.

AUTHOR CONTRIBUTIONS

H.Y.K. designed research, performed experiments, analyzed data and wrote the paper. M.A.Y. designed research, performed experiments, analyzed data and wrote the paper. K.K.H.N., and S.S.P. performed experiments. S.S.D., G.F. and I.D.B. provided reagents. J.A.Z. performed experiments and analyzed data. S.S. analyzed data. M.B.E. designed research. E.V.R. designed research, analyzed data and wrote the paper.

COMPETING FINANCIAL INTERESTS

The authors declare no competing financial interests.

1. Rothenberg, E.V. T cell lineage commitment: identity and renunciation. *J. Immunol.* **186**, 6649–6655 (2011).
2. Yui, M.A. & Rothenberg, E.V. Developmental gene networks: a triathlon on the course to T cell identity. *Nat. Rev. Immunol.* **14**, 529–545 (2014).
3. Avram, D. & Califano, D. The multifaceted roles of Bcl11b in thymic and peripheral T cells: impact on immune diseases. *J. Immunol.* **193**, 2059–2065 (2014).
4. Ciofani, M. *et al.* A validated regulatory network for Th17 cell specification. *Cell* **151**, 289–303 (2012).
5. Liu, P., Li, P. & Burke, S. Critical roles of Bcl11b in T-cell development and maintenance of T-cell identity. *Immunol. Rev.* **238**, 138–149 (2010).
6. Li, L., Leid, M. & Rothenberg, E.V. An early T cell lineage commitment checkpoint dependent on the transcription factor Bcl11b. *Science* **329**, 89–93 (2010).
7. Ikawa, T. *et al.* An essential developmental checkpoint for production of the T cell lineage. *Science* **329**, 93–96 (2010).
8. Wakabayashi, Y. *et al.* Bcl11b is required for differentiation and survival of αβ T lymphocytes. *Nat. Immunol.* **4**, 533–539 (2003).
9. Inoue, J. *et al.* Expression of TCRαβ partly rescues developmental arrest and apoptosis of αβ T cells in *Bcl11b*$^{-/-}$ mice. *J. Immunol.* **176**, 5871–5879 (2006).
10. Li, P. *et al.* Reprogramming of T cells to natural killer–like cells upon *Bcl11b* deletion. *Science* **329**, 85–89 (2010).
11. Yui, M.A., Feng, N. & Rothenberg, E.V. Fine-scale staging of T cell lineage commitment in adult mouse thymus. *J. Immunol.* **185**, 284–293 (2010).
12. Naito, T., Tanaka, H., Naoe, Y. & Taniuchi, I. Transcriptional control of T-cell development. *Int. Immunol.* **23**, 661–668 (2011).
13. Manesso, E., Chickarmane, V., Kueh, H.Y., Rothenberg, E.V. & Peterson, C. Computational modelling of T-cell formation kinetics: output regulated by initial proliferation-linked deferral of developmental competence. *J. R. Soc. Interface* **10**, 20120774 (2013).
14. Guo, Y., Maillard, I., Chakraborti, S., Rothenberg, E.V. & Speck, N.A. Core binding factors are necessary for natural killer cell development and cooperate with Notch signaling during T-cell specification. *Blood* **112**, 480–492 (2008).
15. Weber, B.N. *et al.* A critical role for TCF-1 in T-lineage specification and differentiation. *Nature* **476**, 63–68 (2011).
16. García-Ojeda, M.E. *et al.* GATA-3 promotes T-cell specification by repressing B-cell potential in pro-T cells in mice. *Blood* **121**, 1749–1759 (2013).
17. Scripture-Adams, D.D. *et al.* GATA-3 dose-dependent checkpoints in early T cell commitment. *J. Immunol.* **193**, 3470–3491 (2014).
18. Franco, C.B. *et al.* Notch/Delta signaling constrains reengineering of pro-T cells by PU.1. *Proc. Natl. Acad. Sci. USA* **103**, 11993–11998 (2006).
19. Germar, K. *et al.* T-cell factor 1 is a gatekeeper for T-cell specification in response to Notch signaling. *Proc. Natl. Acad. Sci. USA* **108**, 20060–20065 (2011).
20. Del Real, M.M. & Rothenberg, E.V. Architecture of a lymphomyeloid developmental switch controlled by PU.1, Notch and Gata3. *Development* **140**, 1207–1219 (2013).
21. Panne, D. The enhanceosome. *Curr. Opin. Struct. Biol.* **18**, 236–242 (2008).
22. Spitz, F. & Furlong, E.E. Transcription factors: from enhancer binding to developmental control. *Nat. Rev. Genet.* **13**, 613–626 (2012).
23. Iwafuchi-Doi, M. & Zaret, K.S. Pioneer transcription factors in cell reprogramming. *Genes Dev.* **28**, 2679–2692 (2014).
24. Zhang, D.X. & Glass, C.K. Towards an understanding of cell-specific functions of signal-dependent transcription factors. *J. Mol. Endocrinol.* **51**, T37–T50 (2013).
25. Zhang, J.A., Mortazavi, A., Williams, B.A., Wold, B.J. & Rothenberg, E.V. Dynamic transformations of genome-wide epigenetic marking and transcriptional control establish T cell identity. *Cell* **149**, 467–482 (2012).
26. Wang, H. *et al.* NOTCH1-RBPJ complexes drive target gene expression through dynamic interactions with superenhancers. *Proc. Natl. Acad. Sci. USA* **111**, 705–710 (2014).
27. Yu, M. *et al.* Direct recruitment of polycomb repressive complex 1 to chromatin by core binding transcription factors. *Mol. Cell* **45**, 330–343 (2012).
28. Li, L. *et al.* A far downstream enhancer for murine *Bcl11b* controls its T-cell specific expression. *Blood* **122**, 902–911 (2013).
29. Tydell, C.C. *et al.* Molecular dissection of prethymic progenitor entry into the T lymphocyte developmental pathway. *J. Immunol.* **179**, 421–438 (2007).
30. Mingueneau, M. *et al.* Immunological Genome Consortium. The transcriptional landscape of αβ T cell differentiation. *Nat. Immunol.* **14**, 619–632 (2013).
31. Schmitt, T.M. & Zúñiga-Pflücker, J.C. Induction of T cell development from hematopoietic progenitor cells by Delta-like-1 *in vitro*. *Immunity* **17**, 749–756 (2002).
32. De Obaldia, M.E. & Bhandoola, A. Transcriptional regulation of innate and adaptive lymphocyte lineages. *Annu. Rev. Immunol.* **33**, 607–642 (2015).
33. Weng, A.P. *et al.* c-Myc is an important direct target of Notch1 in T-cell acute lymphoblastic leukemia/lymphoma. *Genes Dev.* **20**, 2096–2109 (2006).
34. Kueh, H.Y., Champhekar, A., Nutt, S.L., Elowitz, M.B. & Rothenberg, E.V. Positive feedback between PU.1 and the cell cycle controls myeloid differentiation. *Science* **341**, 670–673 (2013).
35. Varnum-Finney, B. *et al.* Immobilization of Notch ligand, Delta-1, is required for induction of Notch signaling. *J. Cell Sci.* **113**, 4313–4318 (2000).
36. Schmitt, T.M., Ciofani, M., Petrie, H.T. & Zúñiga-Pflücker, J.C. Maintenance of T cell specification and differentiation requires recurrent notch receptor-ligand interactions. *J. Exp. Med.* **200**, 469–479 (2004).
37. Taghon, T.N., David, E.S., Zúñiga-Pflücker, J.C. & Rothenberg, E.V. Delayed, asynchronous, and reversible T-lineage specification induced by Notch/Delta signaling. *Genes Dev.* **19**, 965–978 (2005).
38. Hosokawa, H. *et al.* Gata3/Ruvbl2 complex regulates T helper 2 cell proliferation via repression of Cdkn2c expression. *Proc. Natl. Acad. Sci. USA* **110**, 18626–18631 (2013).
39. Yu, S. *et al.* The TCF-1 and LEF-1 transcription factors have cooperative and opposing roles in T cell development and malignancy. *Immunity* **37**, 813–826 (2012).
40. Kawazu, M. *et al.* Functional domains of Runx1 are differentially required for CD4 repression, TCRβ expression, and CD4/8 double-negative to CD4/8 double-positive transition in thymocyte development. *J. Immunol.* **174**, 3526–3533 (2005).
41. Zarnegar, M.A., Chen, J. & Rothenberg, E.V. Cell-type-specific activation and repression of PU.1 by a complex of discrete, functionally specialized cis-regulatory elements. *Mol. Cell. Biol.* **30**, 4922–4939 (2010).
42. Peter, I.S. & Davidson, E.H. *Genomic Control Process: Development and Evolution* (Academic Press, 2015).
43. Takahashi, K. & Yamanaka, S. Induction of pluripotent stem cells from mouse embryonic and adult fibroblast cultures by defined factors. *Cell* **126**, 663–676 (2006).
44. Ebina, W. & Rossi, D.J. Transcription factor-mediated reprogramming toward hematopoietic stem cells. *EMBO J.* **34**, 694–709 (2015).
45. Lin, Y.C. *et al.* Global changes in the nuclear positioning of genes and intra- and interdomain genomic interactions that orchestrate B cell fate. *Nat. Immunol.* **12**, 1196–1204 (2012).

ONLINE METHODS

Constructs. Gene-targeting vectors for reporter insertion into *Bcl11b* were generated using a bacterial artificial chromosome (BAC) recombineering method[46], involving two major steps. First, a modified BAC containing the fluorescent reporter to be inserted into the *Bcl11b* locus was generated. An internal ribosome entry site (IRES)-histone 2B-mCitrine yellow fluorescent protein (YFP) cassette was joined to a *loxP*-flanked kanamycin/neomycin (*neo*) drug selection cassette using fusion PCR and inserted into a cloning vector (pGEM-T Easy, Promega). Additional 5′ and 3′ homology arms to the 3′ untranslated region (UTR) of *Bcl11b* were then attached to this IRES-YFP-*neo* cassette through an additional round of fusion PCR. The resultant linear fragment was then inserted into a BAC containing the entire *Bcl11b* gene locus (RP24-282D6, from http://bacpac.chori.org) using a recombineering-competent bacterial strain (SW102)[46]. Correctly targeted BACs were then selected using kanamycin and verified using PCR and pulse-field gel electrophoresis.

Second, targeting sequence from the reporter-modified BAC was retrieved. To generate a retrieval vector, homology regions for the ends of the short and long arms of the targeting vector were joined by fusion PCR, and ligated into a starting ampicillin-resistant vector (PL253)[46] using the restriction enzymes NotI and SpeI (New England Biolabs). Targeting sequence from the modified BAC was then retrieved into this vector using recombineering in SW102 cells, and resultant targeting vectors were selected using kanamycin and ampicillin. In performing this reaction, it was discovered that a 430-bp sequence in the PL253 vector (between the restriction enzymes NotI and DraIII) recombined with the fluorescent protein cassette to generate an undesired side product; this region was removed by excision using NotI and DraIII followed by ligation using a bridging oligonucleotide containing these adjacent sites for these two restriction enzymes.

Banshee retroviral constructs were used as a starting point for constructing shRNA knockdown vectors[17]. To minimize interference in detection of Bcl11b-YFP fluorescence, we first made a mCherry-expressing shRNA retroviral backbone (Banshee-mCherry), by modifying the existing GFP-based shRNA knockdown vector (Banshee-GFP) using PCR cloning[47]. shRNA targeting sequences for *Tcf7*, *Gata3* or *Runx1* or a random sequence were then joined to a U6 promoter by oligonucleotide synthesis and cloned into this Banshee-mCherry backbone using the restriction enzymes BglII and HindIII. Hairpin sequences for these vectors are provided in **Supplementary Table 3**.

Retroviral overexpression constructs were made from a previously generated mCherry-expressing backbone (MSCV-IRES-mCherry)[34], which was based on the NGFR derivative of the pMIGR1 retroviral vector (kindly provided by L. Xu and W. Pear). Full-length Runx1 and the Runx dominant-negative constructs[48] were cloned upstream of the IRES sequence of this vector using the restriction enzymes BglII and EcoRI. The histone-2B mCherry construct was inserted into the MSCV-NGFR vector using PCR cloning with the restriction enzymes BglII and EcoRI. Full-length c-Myc was also inserted into the MSCV-IRES-mCherry vector by PCR cloning with the same restriction enzymes, using as a template a c-Myc retroviral construct from Addgene (13375)[43]. All constructs were verified by sequencing. TCF-1 overexpression constructs and corresponding empty vector controls (MSCV-VEX-GFP) were kindly provided by A. Bhandoola.

To generate nonfluorescent OP9-DL1 cells for live-cell imaging, we generated a pMX-DL1-IRES-hCD8 retroviral construct for transduction into OP9 cells. This was achieved by PCR cloning of mouse DL1 from a cDNA clone (GenBank BC057400) into the pMX-IRES-hCD8 backbone (gift from N. Masuyama) using the restriction enzyme XhoI.

Generation of Bcl11b-YFP knock-in reporter mice. The IRES-YFP-neo cassette was knocked into the endogenous *Bcl11b* locus of V6.5 ES cells through gene-targeting vector transfection, followed by selection of individual neomycin/G418-resistant clones. Correctly targeted clones were identified by PCR and Southern blot analysis (**Supplementary Fig. 2b**) and injected into tetraploid blastocyst embryos. Chimeric founder animals were then crossed to C57/BL6 mice, and offspring containing the knock-in reporter were then bred to homozygosity for this allele. To delete the *loxP*-flanked neomycin cassette from this reporter allele, *Bc11b*$^{YFP/YFP}$ animals were bred to the EIIA-Cre mouse strain (B6.FVB-Tg(EIIa-cre)C5379Lmgd/J, Jackson Labs), which expresses Cre recombinase in the germline. Offspring with a deleted neomycin cassette were identified using PCR and bred to homozygosity for this allele. For *in vitro* assays with BM progenitors, *Bc11b*$^{YFP/YFP}$ mice were crossed to *Bcl2* transgenic mice (B6.Cg-Tg(BCL2)25Wehi/J, Jackson Labs) to obtain offspring heterozygous for both alleles; the *Bcl2* transgene was used to enhance cell survival in these assays. As V6.5 ES cells represent a hybrid between C57/BL6 and 129/Sv strains, we estimate that mice used for our experiments have a small (<12.5%) contribution from the 129/Sv genome. Both male and female animals were used as cell sources, as we did not observe and sex-specific differences in our results. Spleen and thymus were harvested from 4- to 6-week-old mice, whereas BM was harvested from 2- to 3-month-old mice. All animals were bred and maintained in the California Institute of Technology Laboratory Animal Facility, under specific pathogen free conditions, and the protocol supporting animal breeding for this work was reviewed and approved by the Institute Animal Care and Use Committee of the California Institute of Technology.

Analysis of cell populations from thymus and spleen. To analyze Bcl11b-YFP expression in different cell populations, mice were sacrificed, thymi or spleens were dissected, and single-cell suspensions were made. For later-stage precursors (ISP, DP, CD4$^+$, CD8$^+$ in the thymus), and for mature populations (CD8$^+$, CD4$^+$, CD4$^+$CD25$^+$, γδT, NKT, B, NK in the spleen), thymocyte or splenocyte cell suspensions were directly stained using antibodies to cell surface markers (**Supplementary Table 4**) and analyzed using a benchtop flow cytometer (MacsQuant, Miltenyi). For earlier stage precursors (ETP, DN2a, DN2b, DN3, DN4), mature cells were depleted from thymocyte suspensions by staining with biotinylated antibodies to mature cell markers and removal with streptavidin-conjugated magnetic beads before staining with fluorochrome-conjugated antibodies, as previously described[11]. Antibodies used for this analysis are all standard, commercially available monoclonal reagents with widely established use to characterize immune cell populations in the mouse; details are given in **Supplementary Table 4**.

***In vitro* generation of T cell progenitors from bone marrow.** DN T cell progenitors were obtained through *ex vivo* expansion of BM stem and progenitor cells on OP9-DL1 co-cultures, following previously described procedures[17,20,49] with minor modifications. Briefly, BM was removed from the femur and tibia of 2–3-month-old *Bc11b*$^{YFP/+}$ mice. Suspensions of BM cells were then prepared, stained for lineage markers using biotin-conjugated lineage antibodies (CD11b, CD11c, Gr1, TER-119, NK1.1, CD19, CD3), incubated with streptavidin-coated magnetic beads (Miltenyi Biotec), and passed through a magnetic column (Miltenyi Biotec). Lineage-depleted (Lin$^-$) cells were eluted and stored in liquid nitrogen in freezing media (50% FBS, 40% αMEM, 10% DMSO) for future use. To facilitate their development into the DN2 stage, frozen BM cells were thawed and cultured on OP9-DL1 monolayers[31] using standard culture medium (80% αMEM (Gibco), 20% HyClone FBS (Thermo Scientific), Pen Strep Glutamine (Gibco), 50 μM β-mercaptoethanol (Sigma-Aldrich)) supplemented with 5 ng/ml IL-7 and 5 ng/ml Flt3L (Peprotech). To isolate T cell progenitors, cultured cells were directly sorted after 7 d or transduced with retroviral constructs 1 d before sorting. T cell precursor subsets were sorted from the cultures using c-Kit, CD44, and CD25 to approximate as closely as possible ETP, DN2a, and DN2b phenotypes found in thymus. However, because the levels of c-Kit expression on these cultured T cell precursors do not split populations as sharply as those found *in vivo*, we refer to these BM-derived subsets as ETP, Bcl11b-YFP$^-$ DN2, and Bcl11b-YFP$^+$ DN2, respectively.

For retroviral transduction, cultured cells were disaggregated, filtered through a 40-μm nylon mesh, transferred onto RetroNectin/DL1-coated virus bound plates prepared as described below, and cultured with standard medium supplemented with 5 ng/ml IL-7, 5 ng/ml Flt3L, and 5 ng/ml SCF.

For sorting, cells were stained with CD45, CD44, c-Kit, CD25, and a biotin-conjugated lineage cocktail (CD11b, CD11c, Gr1, TER-119, NK1.1, CD19, CD3) (**Supplementary Table 4**), and were sorted for ETP progenitors (Lin$^-$CD45$^+$c-Kit^{hi}CD44^{hi}CD25$^-$) or DN2 progenitors (Lin$^-$CD45$^+$c-Kit^{hi}CD44^{hi}CD25$^+$). DN2 progenitors were further subdivided according to their level of c-Kit expression (Kit^{++} = DN2a, Kit$^+$ = DN2b) and/or their level of Bcl11b-YFP expression (**Figs. 1–7**), and cells transduced with retrovirus were further isolated as mCherry$^+$ cells (**Figs. 4,5,7** and **8**).

doi:10.1038/ni.3514

For cell proliferation experiments (**Fig. 3**), sorted cells were further incubated with 5 μM CellTrace Violet cell proliferation dye (Invitrogen) at 37 °C for 10 min before culture. The small molecule CDK4/6 inhibitor PD0332991 (Selleck Chemicals) was added to culture medium at a final concentration of 2.1 μM in 0.02% DMSO[34].

***In vitro* developmental assays.** Thymus or BM-derived DN progenitors were seeded onto monolayers of OP9-GFP or OP9-DL1-GFP feeder cells[31] and cultured in standard medium supplemented with 5 ng/ml IL-7, 5 ng/ml FLt3L and 5 μm β-mercaptoethanol unless otherwise indicated. In alternate-lineage-potential assays (**Figs. 2a** and **2c**), a fixed number of cells was deposited by the cell sorter into 96-well plates as indicated; for the other assays, cells were first sorted into tubes and distributed manually. Cells were then cultured for the indicated amounts of time then harvested for flow cytometry. For analysis, cells were stained for CD45, CD25 and other antibodies as indicated (**Figs. 3**,**4**,**6**–**8** and **Supplementary Figs. 5** and **7**), or with CD11c, NK1.1 and DX5 for alternate-lineage-potential assays (**Fig. 2**). Stained cells were then analyzed using either the MacsQuant flow cytometer or the MacsQuant VYB flow cytometer for detection of mCherry fluorescence by 561-nm laser excitation. For feeder-free cultures (**Fig. 6**), BM-derived progenitors were cultured directly onto DL1-coated plates, prepared as a described above, with standard medium supplemented with 5 ng/ml SCF, IL-7 and Flt3L, and 5 μM β-mercaptoethanol.

For live imaging, *in vitro* developmental assays were modified in two ways. First, non-GFP-expressing OP9 cells (either OP9 parental cells[50] or OP9-DL1-hCD8 cells described above) were used, to minimize interference in detection of the Bcl11b-YFP fluorescence signal. Second, we attached PDMS micromesh arrays (250-μm diameter, Microsurfaces) to the surface of glass-bottomed 24-well plates (Mattek); these arrays contain small microwells that confine OP9 cells and T cell progenitors to a single imaging field of view on 40× objective (**Supplementary Fig. 4**). OP9 cells and sorted progenitors were then seeded into microwells at appropriate densities to enable cell tracking and prevent cell crowding (~8/well and 1/well, respectively).

To facilitate automated cell tracking in movies, cells were marked with constitutively expressed fluorescence markers in two ways. The first was infection with H2B-mCherry expressing retrovirus (**Fig. 5** and **Supplementary Fig. 4b**), in which sorted cells were seeded onto virus-coated plates and cultured in standard medium with 5 ng/ml SCF, IL-7, and Flt3L. After 8 h of infection, cells were transferred onto OP9-DL1 monolayers in microwells, and then subject to time-lapse live-cell imaging. The second was *in situ* staining with a fluorescence-conjugated antibody to the pan-hematopoietic cell marker CD45. Following a previously described procedure[51], 50 ng/ml CD45-APC was added to the culture medium for imaged cells. In separate experiments, we verified with flow cytometry that direct addition of this antibody to culture medium did not affect the T cell development at these stages (data not shown).

Isolation, activation and transduction of peripheral T cells. To purify peripheral T cells from spleen, we incubated splenocytes with biotin-conjugated antibodies to CD4 and CD8, followed by streptavidin-coated magnetic beads (Miltenyi Biotec), then passed them through a magnetic column. Trapped $CD4^+$ or $CD8^+$ cells were then eluted, and activated by culture with anti-TCRβ (plate-immobilized, 1 μg/ml coating concentration) and anti-CD28 (in solution, 1 μg/ml) for 1 d. After activation, cells were transferred onto RetroNectin- and virus-coated plates for retroviral transduction. After 3 d, cells were resuspended, stained with a fluorescence-conjugated anti-CD8 and analyzed by flow cytometry. In these experiments, cells were cultured in lymphocyte medium (RPMI supplemented with 10% FBS, penicillin–streptomycin–glutamine, nonessential amino acids, sodium pyruvate, and β-mercaptoethanol) supplemented with 100 U/ml IL-2 (Peprotech). **Figure 8d** shows results for $CD8^+$ cells while **Supplementary Figure 8b** shows those for $CD8^-$ ($CD4^+$) cells, because CD8 surface levels are more stable under these stimulation conditions.

Statistical analysis of alternate lineage potential. In alternate-lineage-potential assays, wells seeded with low numbers of starting precursors (input numbers) were first scored for NK cell or DC development using flow cytometry and the markers NK1.1-DX5 for NK cells and CD11c for DC (**Fig. 2a**,**c**). A model, logistic in log of starting cell number, was fit, and the probability of a positive well from 10 cells was taken as a measure of developmental potential. The effect of Bcl11b-YFP activation on developmental potential was estimated as the difference of these probabilities, and tested by comparing the difference to its standard error using a *z*-statistic.

Sample preparation for RNA-seq. Total RNA was extracted from 1 million–2.5 million cells using TRIzol (Invitrogen) and subjected to two rounds of selection using oligo-dT-coupled magnetic beads (Dynabeads) according to the manufacturer's protocol. About 50–100 ng polyadenylated mRNA per sample was obtained after double selection. RNA was fragmented to an average length of 200 bp by Mg^{2+}-catalyzed hydrolysis and then converted into cDNA by random priming. cDNA was then subjected to end repairing, adaptor ligation, size selection and one round of PCR amplification.

Analysis of RNA-seq data. RNA-seq data were analyzed with an established analysis pipeline consisting of the programs TopHat and Cufflinks[52], and output data were further analyzed and visualized using MATLAB. Briefly, reads from the sequencer were mapped onto the *mm9* reference mouse genome (NCBI build 37) using TopHat. Gene-expression values, in fragments per kilobase-million (FPKM) were then obtained, and differential expression analysis with replicate biological data was then performed using the statistical model from the Cufflinks software.

For principal component analysis (PCA) of developmental trajectories (**Fig. 2d**), we first obtained the set of all differentially expressed genes across the ETP (DN1), DN2a and DN2b stages from a previous study[25] using pairwise comparisons with a probabilistic cutoff of $P < 0.002$. FPKM values for these genes from both the past study and the current work were log-transformed and normalized across all conditions, with normalizations performed separately for these two data sets to prevent nondevelopmental differences in gene expression from obscuring the PCA analysis. Projections and loadings along the first two principal components were then plotted (**Fig. 2d**).

For analysis of gene-expression changes during *Bcl11b* activation, we either started with a list of genes that were differentially expressed upon *Bcl11b* activation ($P < 0.005$, between Bcl11b-YFP^- and Bcl11b-YFP^+ DN2 cells, **Fig. 2e** and **Supplementary Table 1**), or with a manually selected list of regulatory genes known to be important for T cell development (**Fig. 2e** and **Supplementary Table 2**). Weakly expressed genes with a total count <5 were then excluded, and remaining genes were subject to a hierarchical clustering using an unweighted average distance metric. Computed clusters were then visualized using heat maps (**Fig. 2e**).

Retroviral transduction and preparation of the DL1-coated plates. Viral particles were generated by transient cotransfection of the Phoenix-Eco packaging cell line with the retroviral construct and the pCL-Eco plasmid (Imgenex). Viral supernatants were harvested at 2 and 3 d after transfection and immediately frozen at −80 °C until use. For experiments involving retroviral transduction, tissue culture plates (Costar, Corning) were incubated overnight with 33 μg/ml RetroNectin (Clontech) and 2 μg/ml of the DL1 extracellular domain fused to human IgG1 Fc (DL1-Fc protein), and then loaded with viral supernatant. Cells were then cultured directly on virus-bound plates under the conditions described below. For experiments involving culture of sorted progenitors on DL1-coated plates (**Fig. 6**), tissue culture plates (Costar, Corning) were coated by incubation overnight with 33 μg/ml RetroNectin (Clontech) with different concentrations of the DL1-Fc protein.

Generation of OP9-DL1-hCD8 cell lines. OP9 cells[50] were transduced with DL1-IRES-hCD8 retrovirus, and single hCD8-expressing cell clones were generated by sorting low, limiting numbers of $hCD8^+$ cells onto 96-well plates. Individual clones of OP9-DL1-hCD8-infected cells were then assayed for their ability to support T cell development and survival, and working clones were then expanded, frozen and used for subsequent experiments.

Live-cell imaging. Long-term time-lapse imaging of cultured tells was performed using a previously described method with some modifications[34]. Briefly, imaging was performed on a motorized inverted fluorescence microscope (IX-81, Olympus) using a 40×/0.95 NA oil objective (**Supplementary**

Fig. 4). The microscope was fitted with laser-based focus drift correction (ZDC, Olympus) to maintain a constant plane of imaging and also fitted with a custom-built incubator to maintain a constant humidified environment at 37 °C with 7% CO_2. Images of cultured cells were acquired at fixed time intervals in the differential interference contrast (DIC), YFP, and mCherry or APC channels using image acquisition software (Metamorph, Molecular Devices). Shorter time-lapse intervals (3 min) were for DIC image acquisition, whereas longer time-lapse intervals (15 min) were used for acquisition of fluorescence images to minimize phototoxicity. At each time interval, multiple microwells within the microwell array were visited using a motorized X-Y stage (ASI Scientific). To correct for uneven fluorescence illumination, tiled images of uniformly fluorescent beads (Tetraspeck beads, Invitrogen) were acquired in the same fluorescence channels and processed to generate a correction matrix as described[34].

Image segmentation and analysis. Cells were segmented and tracked using custom image processing workflow implemented in MATLAB (Mathworks), as described[34]. Briefly, this workflow involved the following steps: first, images were corrected for uneven illumination correction and background subtracted. A matrix for correcting uneven illumination was calculated from fluorescent bead images, and applied to the fluorescence images. Corrected images were then subtracted for background using a top-hat filter. Second, cells were subject to automated segmentation. Images were smoothed using Gaussian filtering, run through a Laplacian filter to detect fluorescence object boundaries, and thresholded. Resultant closed object boundaries were then filled to generate solid segmented objects and then subject to size and shape selection to identify cells. Third, cells were tracked automatically. Objects from adjacent movie frames were matched using the Munkres assignment algorithm, using an objective function that incorporates differences in Euclidean distance, shape and object brightness. This automated tracking procedure generates single-cell time traces, which then need to be manually checked and corrected for errors. Fourth, cells that were automatically segmented and tracked were then subject to manual refinement to identify missed cells, split touching cells, and label cell division events. For one of the imaging data sets (**Fig. 5**), we performed manual refinement on cell segmentation but did not further refine automated cell tracking results, nor did we further utilize tracking information for subsequent analysis. To expedite these corrections, we developed a MATLAB graphical user interface that allows a user to review and edit objects and tracks from a time-lapse movie.

Code availability. Image analysis code is available upon request to H.Y.K.

46. Liu, P., Jenkins, N.A. & Copeland, N.G. A highly efficient recombineering-based method for generating conditional knockout mutations. *Genome Res.* **13**, 476–484 (2003).
47. Hernández-Hoyos, G., Anderson, M.K., Wang, C., Rothenberg, E.V. & Alberola-Ila, J. GATA-3 expression is controlled by TCR signals and regulates CD4/CD8 differentiation. *Immunity* **19**, 83–94 (2003).
48. Telfer, J.C., Hedblom, E.E., Anderson, M.K., Laurent, M.N. & Rothenberg, E.V. Localization of the domains in Runx transcription factors required for the repression of CD4 in thymocytes. *J. Immunol.* **172**, 4359–4370 (2004).
49. Champhekar, A. *et al.* Regulation of early T-lineage gene expression and developmental progression by the progenitor cell transcription factor PU.1. *Genes Dev.* **29**, 832–848 (2015).
50. Nakano, T., Kodama, H. & Honjo, T. Generation of lymphohematopoietic cells from embryonic stem cells in culture. *Science* **265**, 1098–1101 (1994).
51. Schroeder, T. Long-term single-cell imaging of mammalian stem cells. *Nat. Methods* **8** (suppl.), S30–S35 (2011).
52. Trapnell, C. *et al.* Differential gene and transcript expression analysis of RNA-seq experiments with TopHat and Cufflinks. *Nat. Protoc.* **7**, 562–578 (2012).

doi:10.1038/ni.3514